THE NONSYNCHRONOUS WHIRLS OF THE TURBINE ROTOR IN AEROJET ENGINES ICAS-82-4.4.1

Gu Jia-Liu, Associate Professor, and Ren Pin-Zhen, Lecturer
Northwestern Polytechnical University
Xian, China

Abstract

Through full-scale engine vibration studies in recent years, we found that in a number of the engines tested there existed the phenomenon of 1/2 order sub-harmonic vibration (the half-frequency whirl), which often became the major cause of excessive vibration level in test. This is a phenomenon of non-linear self-excited vibration. If we can find out its cause and inhibit or eliminate it, the mechanical performance of such a type of engine can certainly be improved.

Based on the characteristics of the nonsynchronous whirls as shown in engine vibration spectra and taking into account the details of construction of the engine, this paper analyses four possible major causes of self-excited vibration: the unbalanced torque force due to circumferential variations of blade tip clearances, the aero-elastic effect of the radial clearances of labyrinth seal, the frictional force within the splined coupling, and the nonlinear stiffness of the supports.

This paper summarizes briefly the 1/2 order sub-harmonic vibration phenomena observed in engine test, and taking the overhung rotor as the mathematical model, deduces its dynamic equations to take into account the effect of the four above-mentioned major factors.

It must be acknowledged that much previous work has been done on the analysis of destabilizing factors. But previous work generally employs a Jeffcott rotor and studies each of the destabilizing factors separately.

This paper discusses the destabilizing factors in connection with a specific type of aircraft engine, and studies the dynamics of the overhung low-pressure turbine rotor under the combined action of these factors for the purpose of explaining the phenomena observed in the spectra of engine vibrations.

Investigations show that the frictional force within the splined coupling is the most important cause of self-excited vibration, and the non-linear stiffness of the back support is responsible for transforming the self-excited vibration into autotracking 1/2 order sub-harmonic whirl. The theoretical results of numerical calculation and those obtained from an analogue computer can be successfully used to explain the various kinds of non-synchronous whirls observed in tests.

It is also the intent of this paper to discuss the possibility of improving system stability by modification of labyrinth (comb-type) seal, and to suggest measures for inhibiting 1/2 order sub-harmonic whirl.

The phenomena of 1/2 order sub-harmonic vibration within aerojet engines

Real-time digital spectral analysis of rig test data taken from vibration recording magnetic tapes for 18 engines showed that 8 of them exhibited the phenomena of 1/2 order sub-harmonic vibration. A typical spectrum (PSD) is illustrated in figure 1.

From the results of spectral analysis we found that:

1. The 1/2 order sub-harmonic vibration is "auto-tracking and precise", i.e. the ratio of the non-synchronous precession speed of rotor to its rotating speed is strictly 0.5 , and it holds constant when rotating speed changes.

2. The 1/2 order sub-harmonic vibration appears only in a relatively narrow speed range, and reaches its maximum at a certain speed.

3. When the 1/2 order (half-frequency) component reaches its maximum, it often exceeds the fundamental component, thus becoming the major cause of excessive vibration level in engine rig tests. The alternating stresses produced within the rotor by the non-synchronous precession contributes also to making it more dangerous than the fundamental component.

4. The 1/2 order component measured at the turbine case is greater than that measured at the compressor case.

The low-pressure turbine rotor of this type of engine operates in the supercritical regime. This is also a necessary condition for the appearance of self-excited vibration.

The causes of 1/2 order sub-harmonic vibration

Instability of high speed rotors has been one of the major research areas in rotor dynamics for more than half a century. It is also a difficult problem frequently encountered by engineers in the production and operation of high speed rotating machinery. Excellent surveys discussed the causes and mechanisms of self-excited vibrations, and gave extensive lists of references.[1-5]

Comparing the characteristics of non-synchronous whirls caused by various factors with the phenomena of 1/2 order sub-harmonic vibration summarized as above, and considering the specific structural features of these aerojet engines, we can visualize such a self-excitation process as follows :

If, when the running speed is somewhat higher than the first critical speed of the rotor, an initial non-synchronous precession for some accidental reason occurs, then the frictional moment within the splined coupling, the circumferential variations of blade tip clearances and the aero-elasticity of labyrinth seals can each contribute to the formation of destabilizing forces which maintain and promote the non-synchronous precession, thus causing a self-excited vibration. The frequency of non-synchronous precession is nearly equal to the first natural frequency of the rotor, and the ratio of the former to rotor speed is at first approximately equal to 0.5 . Due to the effect of subharmonic synchronization, there occurs an auto-tracking 1/2 order precession[6]. The cause of this effect may be the non-linear stiffness of the supports.

Alternatively it is also possible that the non-linear stiffness of the support first creates a 1/2 order sub-harmonic vibration in some of the speed region, which then induces the forces mentioned above to maintain and promote the nonsynchronous precession, thus making the rotor precess under the combined action of several factors.

Mathematical expressions for destabilizing forces

1. The unbalanced torque force due to circumferential variations of blade tip clearances

The results of Alford's research on this question more than a decade ago are still widely accepted.[7,8] The unbalanced torque force (a system of tangential forces) due to circumferential non-uniformity of the blade tip clearances is equivalent to a resultant force causing the forward precession of the rotor. It can be expressed as

$$F_b = \frac{\beta M_t}{2 r_p h}\delta_r \qquad (1)$$

where δr is the radial deflection of the impeller, Mt is the torque of the stage, rp is pitch radius, h is blade height, and β, representing the value of $\Delta\eta_T/(\delta_r/h)$, is a coefficient usually with a numerical range of 1-1.5 , η_T is the stage efficiency.

Because F_b is 90 deg ahead of the deflection δ_r , it corresponds to a gas-dynamic cross-coupled force acting in the disk plane, and the gas-dynamic cross-coupled stiffness in the same plane can be represented by (see fig. 2a)

$$Q = -K_{xy} = K_{yx} = \frac{\beta M_t}{2 r_p h} \qquad (2)$$

2. The frictional moment within splined coupling

When the rotor operates in the super-critical condition, the frictional moment within splined coupling can contribute to maintaining and promoting the forward nonsynchronous precession. This frictional moment is

$$M_f = 0.636 \mu M_t \qquad (3)$$

where μ is the dry coefficient of friction, normally with numerical range of 0.15-0.25[9,10]

This frictional moment is equivalent to a force acting on the disk and causing forward precession

$$F_S = M_f / L \qquad (4)$$

where L is the distance between coupling and disk.

3. The aero-elasticity of labyrinth seals

The aero-elastic effect of labyrinth seals, depending on whether its clearance is divergent or convergent in the direction of flow, will create a force contributing to the stabilization or destabilization of the rotor.[7]

Starting from the analysis in ref. 11, we have derived the expressions for aero-elastic force in the case of a multi-blade seal when the rotor performs a general precession.

It is assumed that, when $t \leqslant 0$, the rotor motion is a forward synchronous precession, and that self-excited whirl is initiated at t=0. Then the expressions for aero-elastic forces FL_x , FL_y, due to circumferential variations of the clearance in labyrinth seal, are derived as follows.

Using the relations given by ref. 11, we have

$$\Delta P_i(\theta, t) = \frac{d(\Delta P_i(\theta, t))}{dt} = \frac{d\tilde{P}_i(\theta, t)}{dt} \qquad (5)$$

Substituting certain appropriate relations (omitted in this paper) into equation (5), we obtain

$$\Delta P_i(\theta, t) = \frac{RT_0}{V_i}[-A_i \Delta P_i(\theta, t) - B_i(x\cos\theta_i + y_i \sin\theta_i)] \quad (i=1, z.....z-1) \qquad (6)$$

where Z=the number of teeth,

$A_1 = WP_1/(P_0^2 - P_1^2)$

$A_{z-1} = WP_z^2/[P_{z-1}(P_{z-1}^2 - P_z^2)]$, when the flow is not choked for the final tooth tip clearance, and $A_{Z-1}=0$, when it is choked.

$A_i = 0 \quad (i=2,3 \ldots\ldots Z-2)$,

V_i=Volume of ith cavity per unit length of circumference,

X_i, Y_i = instantaneous deflections of ith cavity in X, Y direction respectively,

θ =Position of the circumferential element of unit length being analyzed, i.e. its angle measured from X axis,

W= steady-state absolute static pressure within ith cavity,

$\tilde{P}_i(\theta,t)=P_i+\Delta P_i(\theta,t)$ instantaneous absolute static pressure at position within ith cavity,

R= gas constant,

$\beta_i=\frac{W}{\delta_i}(1-\frac{\delta_i}{\delta_{i+1}})$, here δ_i - static clearance at ith tooth tip, T_0=total temperature.

Then we obtain

$$FL_X=-\sum_{i=1}^{z-1}\int_0^{2\pi}\Delta P_i(\theta,t)R_iS_0\cos\theta\,d\theta \quad (7)$$

where Ri is the root radius of seal, s_0 is the distance between consecutive teeth.

Let radial deflection be Xi, then

$$\left.\begin{aligned} x_i&=X_i\cos(\omega t-\phi)\\ y_i&=X_i\sin(\omega t-\phi)\end{aligned}\right\} \quad (8)$$

here ω is the running speed, ϕ_i is the initial phase angle. From equations (6),(7) and (8) we obtain

$$\Delta P_i(\theta,0)=\frac{-RT_0B_iX_i\cos(\phi+\phi_i+\theta)}{\sqrt{V_i^2\omega^2+(RT_0)^2A_i^2}} \quad (9)$$

$$\phi_i=\arctan\frac{V_i\omega}{RT_0A_i} \quad (10)$$

$$FL_i|_{t=0}=\pi R_iS_0\frac{-RT_0B_iX_i}{\sqrt{V_i^2\omega^2+(RT_0)^2A_i^2}} \quad (11)$$

$$\left.\begin{aligned} FL_{ix}|_{t=0}&=FL_i|_{t=0}\cdot\cos(\phi+\phi_i)\cdot x_i(0)/|x_i(0)|\\ FL_{iy}|_{t=0}&=FL_i|_{t=0}\cdot\sin(\phi+\phi_i)\cdot x_i(0)/|x_i(0)|\end{aligned}\right\} \quad (12)$$

When t>0, there occurs self-excited whirl, and the rotor performs a general precession, then it is derived from equation (7) that

$$\frac{dFL_X}{dt}=\sum_{i=1}^{z-1}\frac{dFL_{ix}}{dt} \quad (13)$$

$$\frac{dFL_{ix}}{dt}=-\frac{A_iRT_0}{V_i}FL_{ix}+\frac{B_iRT_0}{V_i}R_iS_0\pi x_i \quad (14)$$

Similarly we obtain

$$FL_y=-\sum_{i=1}^{z-1}\int_0^{2\pi}\Delta P_i(\theta,t)R_iS_0\sin\theta\,d\theta \quad (15)$$

$$\frac{dFL_y}{dt}=\sum_{i=1}^{z-1}\frac{dFL_{iy}}{dt} \quad (16)$$

$$\frac{dFL_{iy}}{dt}=-\frac{A_iRT_0}{V_i}FL_{iy}+\frac{B_iRT_0}{V_i}R_iS_0\pi y_i \quad (17)$$

Equations (14), (17) together with the equations of rotor motion may be solved by numerical integration, and the solution's initial values should be as given by equation (12).

Mathematical expressions for parametric excitation

1. The non-linear stiffness of single-row deep-grooved ball bearing

The radial flexibility of ball bearing originates from the contact deformation between the rolling track and the ball. Based on the analysis in reference 12, the characteristic of the radial stiffness of bearing can be related to the following equation

$$\Delta x=\frac{1}{K}P^n \quad (18)$$

where P is the radial load, Δx is the relative displacement between the inner and outer ring of the bearing under the action of radial load P, the coefficient K depends upon the geometry, dimensions, and material of bearing, the exponent n is 2/3 for the ball bearing, and 0.9 or 1.0 for the roller bearing.

In most aero engines, the elastic constant C_1 of supporting system is usually much smaller that of the bearing itself. In such a case, if the elastic characteristic of the support is linear, then the relation describing the combined spring characteristic of the ball bearing and support can be deduced as follows:

From figure 3 it can be seen that

$$P=k^{3/2}\Delta x^{3/2}=C_1x_2=C_1x_1-\frac{C_1}{k}P^{2/3} \quad (19)$$

Since $x\ll x_2$, P on the right hand side of equation (19) can be approximated by C_1X_1, i.e.

$$P\approx C_1x_1-\frac{C_1}{k}(C_1x_1)^{2/3} \quad (20)$$

The radial load can also be approximated by

$$P^*=C_2x_1+C^*x_1^3 \quad (21)$$

The values of C_2 and C^* can be found from the condition of least squares, i.e.

$$\frac{\partial}{\partial C^*}\left(\text{or }\frac{\partial}{\partial C_2}\right)\int_0^A[P(x_1)-P^*(x_1)]^2dx_1=0 \quad (22)$$

Inserting (20),(21) into (22), we obtain

$$\left.\begin{aligned} C_2&=C_1-1.406\frac{C_1^{5/3}}{k}A^{-\frac{1}{3}}\\ C^*&=\frac{15}{32}\frac{C_1^{5/3}}{k}A^{-2\frac{1}{3}}\end{aligned}\right\} \quad (23)$$

where A is the amplitude.

2. The non-linear stiffness of the back support

The flexibility of turbine shaft case is rather large, and the rigidity of back support is assured by means of transmitting the greater part of the load from back support to turbine case through the long screws and plugs within the stator blades.

The cold radial clearance between the plugs and cases is $+0.217 \sim -0.02$ mm. The clearance diminishes when the engine operates; for most of the plugs the clearance will be negative, but for the rest it may still be positive. Thus the stiffness of back support becomes nonlinear, as shown in figure 4.

Let the instantaneous radial deflection at the moment of t, when the rotor precesses, be r, the deflection obviously occurs in the flexural plane. If the stiffness of the back support is the same in all directions, then the reaction of support

$$\begin{aligned} P&=-[k_1 r_0+(k_1+\triangle k)(r-r_0)] \\ &=-[k_2 r-\delta k_2] \end{aligned} \tag{24}$$

where $k_2=k_1+\triangle k$

$$\delta=\frac{\triangle k}{k_2} r_0$$

r_0 = the clearance when the rotor is running

The reaction components are

$$\left.\begin{aligned} P_x&=P\cos\psi=-(k_2 x-\delta k_2 \cos\psi) \\ P_y&=P\sin\psi=-(k_2 y-\delta k_2 \sin\psi) \end{aligned}\right\} \tag{25}$$

where ψ is the angle of precession.

In fact the stiffness of the back support will be not only nonlinear but also asymmetric, furthermore the nonlinear stiffness will have hardening characteristic. In this case the corresponding expressions can be derived and written as

$$\left.\begin{aligned} -P_x&=k_1' x+\triangle k \cdot x\cos\psi \\ -P_y&=k_1' y+\triangle k \cdot y\sin\psi \end{aligned}\right\} \tag{26}$$

where $k_1'=k_1-2a r_0$

$$P(r)=k_1 r+a(r-r_0)^2$$

here p(r) is the hardening characteristic of nonlinear stiffness of the back support.

The equations of motion of the high-speed overhung turbine rotor

1. Mathematical model

The overhung turbine rotor with dynamic unbalance Ge_1 and moment unbalance Ge_2S, shown in figure 5, is supported by fore and back elastic supports, and subjected to the actions of several factors described above which cause instability and parametric excitation.

The effects of these factors on rotor motion have been discussed in the preceding sections.

As this type of engine is not provided with built-in damping device, the influence of material and structure damping can be considered by means of resonance amplification. The amplification factors of 10-25 are common for aircraft engine rotors supported on undamped antifriction bearings.[7,8] Thus

$$C_{eq_1}\approx\frac{\sqrt{K_{11}m}}{Q_1}, \qquad C_{eq_2}\approx\frac{\sqrt{K_{22}J_d}}{Q_2} \tag{27}$$

where K_{11}, K_{22} (K_{12}) are the stiffness coefficients, m and J_d are the equivalent mass and diametrical moment of inertia of the rotor respectively.

Thus the simplified model for the rotor-supports system has five degrees of freedom.

2. Derivation of the equations of motion

The equations of motion of the turbine rotor can be derived from Lagrange's equations. we used the fixed right hand coordinate system OXYZ, and take the following as the generalized coordinates: the deflections of the center of the impeller X, y (see fig. 6) and its angular displacements $\alpha=\theta_x$, $\beta=\theta_y$ (see fig.7). Then the equations of motion of the overhung turbine rotor under the combined action of several destabilizing factors can be derived, and written as

$$\begin{aligned} &m\ddot{x}+K_{11}\left(1+\bar{\Delta}\frac{x}{\sqrt{x^2+y^2}}\right)x+K_{12}\left(1+\bar{\Delta}\frac{\beta}{\sqrt{\alpha^2+\beta^2}}\right)\beta \\ &+c^*[(a_1x+b_1\beta)^2+(a_1y-b_1\alpha)^2]\cdot(a_1x+b_1\beta)a_1 \\ &=F_{sx}+FL_x+me_1\omega^2\cos\omega t-c_{eq_1}\dot{x}+K_{xy}y \end{aligned} \tag{28}$$

$$\begin{aligned} &m\ddot{y}+K_{11}\left(1+\bar{\Delta}\frac{y}{\sqrt{x^2+y^2}}\right)y-K_{12}\left(1-\bar{\Delta}\frac{\alpha}{\sqrt{\alpha^2+\beta^2}}\right)\alpha \\ &+c^*[(a_1x+b_1\beta)^2+(a_1y-b_1\alpha)^2]\cdot(a_1y-b_1\alpha)a_1 \\ &=F_{sy}+FL_y+me_1\omega^2\sin\omega t-c_{eq_1}\dot{y}+K_{yx}x \end{aligned} \tag{29}$$

$$\begin{aligned} &J_d\ddot{\alpha}+J_p\omega\dot{\beta}-K_{12}\left(1+\bar{\Delta}\frac{y}{\sqrt{x^2+y^2}}\right)y+K_{22}\alpha \\ &-c^*[(a_1x+b_1\beta)^2+(a_1y-b_1\alpha)^2]\cdot(a_1y-b_1\alpha)b_1 \\ &=-me_2s\omega^2\sin(\omega t+\lambda)-c_{eq_2}\dot{\alpha} \end{aligned} \tag{30}$$

$$\begin{aligned} &J_d\ddot{\beta}-J_p\omega\dot{\alpha}+K_{12}\left(1+\bar{\Delta}\frac{x}{\sqrt{x^2+y^2}}\right)x+K_{22}\beta \\ &+c^*[(a_1x+b_1\beta)^2+(a_1y-b_1\alpha)^2]\cdot(a_1x+b_1\beta)b_1 \\ &=me_2s\omega^2\cos(\omega t+\lambda)-c_{eq_2}\dot{\beta} \end{aligned} \tag{31}$$

where Jp=the polar moment of inertia of the impeller,

$$\left.\begin{aligned} F_{sx}&=\frac{-0.636\mu M_t}{L}\cdot\frac{y}{\sqrt{x^2+y^2}}=-F_s\frac{y}{\sqrt{x^2+y^2}} \\ F_{sy}&=F_s\frac{x}{\sqrt{x^2+y^2}} \end{aligned}\right\} \tag{32}$$

$$\left.\begin{aligned} a_1&=\xi_{13}K_{12}+\eta_{13}K_{12} \\ b_1&=\xi_{13}K_{12}+\eta_{13}K_{22} \end{aligned}\right\} \tag{33}$$

here ξ (deflection per unit force), η (deflection per unit moment) are the cross-coupling influence coefficients between the 1 and 3 planes (fig. 8),

$$\bar{\Delta}=\frac{1}{a_{11}}\left(\frac{L}{l}\right)^2\frac{\Delta k}{k_1'^2} \tag{34}$$

$$[a_{ij}]_{2\times 2}=[K_{ij}]_{2\times 2}^{-1}$$

other symbols have been explained previously.

For solving the nonlinear differential equations (14),(17),(28)-(31), we used the numerical integration method (the direct integration method). The calculated results for the turbine rotor of this type of engine are given in Tables 1 and 2.

For saving computing time, we first solved the simplified equations on an analogue computer. The calculated results are shown in figures 9-12. They agree well with the results of numerical calculation shown in figures 13 and 14.

Concluding Remarks

This paper discussed several factors involved in the stability analyses of the supercritical overhung-rotor-bearing system of a specific type of aircraft engine. The authors are of the opinion that, both these factors and the mathematical model used in this paper are applicable to the low-pressure turbine rotors of many other types of engines.

The following tentative conclusions may be drawn :

1. The frictional moment created within the splined coupling, when the running speed of rotor is supercritical, is the most important factor causing the non-synchronous forward precession of the rotor.

2. Depending on the quality of fitting the plugs into cases, the stiffness characteristic of back support under operating conditions may be linear or nonlinear, thus determining the behavior of vibration.

If it is linear, it has no effect on self-excited vibration of the rotor; the whirl frequency, approximately equal to the first natural frequency of the system, varies slightly, so does the whirl amplitude. In such a case the power spectrum of engine casing vibration takes on the nature of a narrow-band random vibration.

If it is nonlinear (i.e. hardening), the self-excited vibration of the rotor is transformed into the 1/2 order sub-harmonic vibration, i.e. the whirl speed ratio approaches and finally reaches 1/2; moreover, such a mode of precession is retained in a relatirely narrow speed range (about 1,000 rpm for this rotor) situated in the supercritical speed region. It is likely to be the sub-harmonic resonance.

3. Taking measures such as adding an intermediate bearing to increase the critical speed of the system is the most effective method for vibration reduction.

4. Keeping the structural details of the engine essentially intact, measures such as the following are effective for vibration reduction: to assure the precision of bearings and the assembly quality of the supports, to reduce the frictional force within the splined coupling, and to obtain proper clearance between the plugs and cases.

5. Making the tooth tip clearance of seal increase from one tooth to the next in the direction of the flow may be a good method for inhibiting the self-excited vibration as shown in Table 2.

This paper seems to succeed in explaining satisfactorily the various kinds of phenomena observed in spectra and recommends some measures for vibration reduction, but the effectiveness of all these measures must be further examined in the full-scale engine tests. This work remains to be done.

References

(1) D.E.Bently: "Forward subrotative speed resonance action of rotating machinery"—— (Proceedings of the 4th Turbomachinery Symposium) P.103 (1976).

(2) E.J.Gunter: "Dynamic stability of rotor-bearing systems"——(NASA-SP-113) (1966).

(3) F.F.Ehrich: "Identification and avoidance of the self-excited vibrations in rotating machinery"—— (ASME 72-DE-21) (1972).

(4) J.M.Vance and A.C.Royal: "High-Speed rotor dynamics—An assessment of current technology for small turboshaft engines"—— (Journal of Aircraft) Vol.12, No.4 (1975).

(5) T.Iwatsubo: "Stability problems on rotor systems"—— (The shock and vibration digest) Vol.11, No.3 (1979).

(6) D.E.Bently: "Forced subrotative speed dynamic motion of rotating machinery"——(ASME 74-PET-16) (1974).

(7) J.S.Alford: "Protecting turbomachinery from self-excited rotor whirl"—— (Trans. ASME—Series A) Vol.87, No.4 (1965).

(8) R.G.Kirk: "The impact of rotor dynamics analysis on advanced turbo compressor design"—— (IME C 181/76) (1976).

(9) R.Williams Jr. and R. Trent : "The effects of nonlinear asymmetric supports on turbine engine rotor stability" —(SAE 700320)(1970).

(10)R.A.Marmol: "Spline coupling induced non-synchronous rotor vibrations"——(ASME 79-DET-60) (1979).

(11)R.T.Murphy and J.M.Vance: "Labyrinth Seal effects on rotor whirl instability"——(IME C306/80) (1980).

(12)Спицын Н.А.: "Опоры осей и валов машин и приборов" — (Машиностроение) (1970).

Table 1 Effect of and e_1 on the response

(Q-20, e_2S-20 mm^2, λ-0, μ-0.25)

		e_1 -0.02 mm					e_1 = 0.04 mm				
res \ ω 1/sec		900	1000	1100	1200	1300	900	1000	1100	1200	1300
$\bar{\Delta}$ -0.05	syn	0.1229	0.1009	0.0881	0.0800	0.0874	0.2431	0.1988	0.1751	0.1555	0.1401
	non-syn	0.0046	0.0030	0.0045	0.0146	0.1355	0.0087	0.0047	0.0067	0.0086	0.0148
	n*	½ order	~665.8	~633.1	~661.4	½ order	½ order	½ order	633.1~678.6	½ order	½ order
$\bar{\Delta}$ -0.1	syn	0.1297	0.0993	0.0881	0.0810	0.0867	0.2438	0.1965	0.1757	0.1574	0.1599
	non-syn	0.0021	0.0055	0.0054	0.0342	0.2146	0.0169	0.0084	0.0081	0.0108	0.0228
		½ lrder	½order	~688.6	~661.4	½ order	½order	½order	~620.1	½ order	½ order
$\bar{\Delta}$ -0.15	syn	0.1248	0.0961	0.0881	0.0818	0.0907	0.2479	0.1898	0.1766	0.1567	0.1380
	non-syn	0.0127	0.0088	0.0046	0.0356	0.2369	0.0257	0.0121	0.0097	0.0131	0.0370
		½ order	½order	~633.1	~676.4	½ order,	½order	½ order	~620.1	½ order	½ order

*ω_n is the angular speed of nonsynchronous whirl

Table 2 Effect of labyrinth seal on the response

ω -1150 1/sec, $\bar{\Delta}$ -0.025 , e_1-0.06 , Q_1-20 , λ -0 , μ -0.15 , δ_o -0.5mm

$\Delta\delta$ (mm)	syn. res (mm)	non-syn. res (mm)	notation
0.0	0.098	0.058	ω -1162.7 1/sec
0.02	0.095	0.034	
0.04	0.1	0.029	
0.06	0.101	0.026	

$$\delta_i=\delta_0+(i-1)\Delta\delta$$

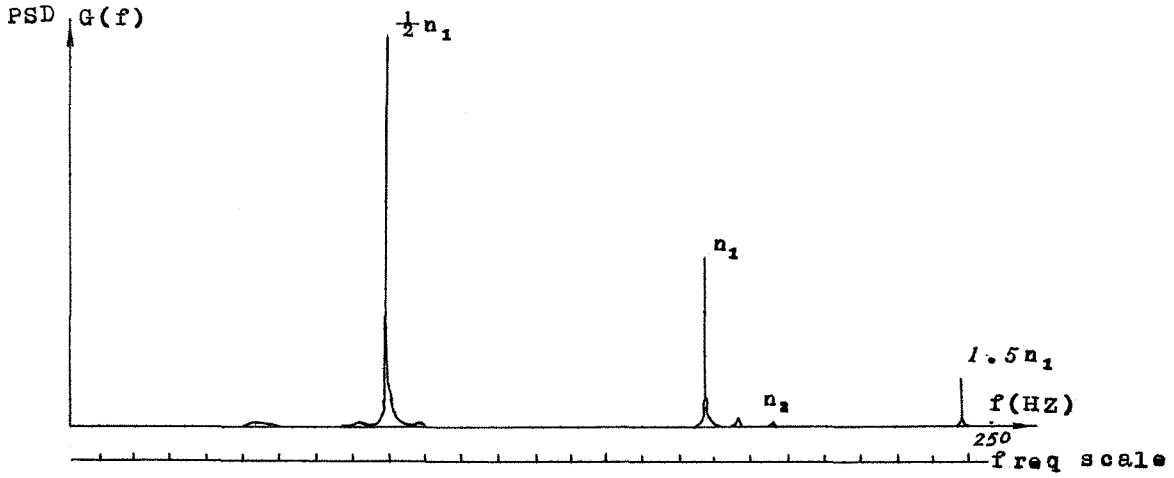

Fig.1 Power spectrum of an engine casing vibration

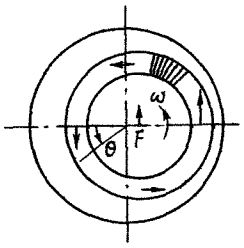

Fig.2a
Phase relation of unbalanced torque force and rotor eccentricity

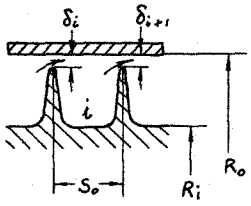

Fig.2b
Aero-elastic action of the radial clearance of labyrinth seal

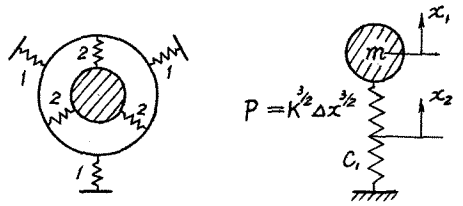

Fig.3 Non-linear stiffness of the fore support

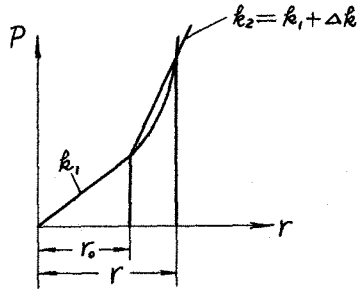

Fig.4
Non-linear stiffness characteristic of the back support

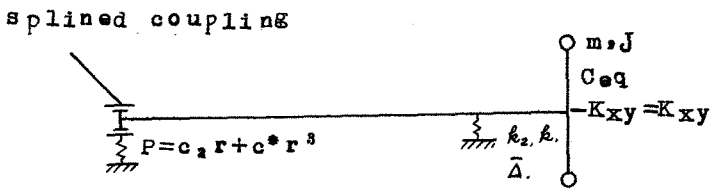

Fig. 5 Simplified model of the overhung turbine rotor

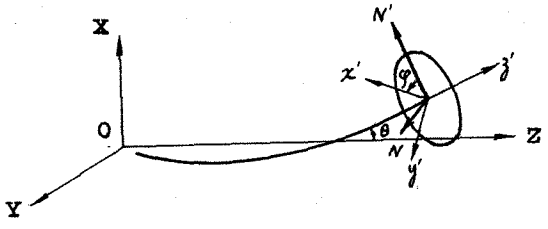

Fig. 6 Generalized coordinates

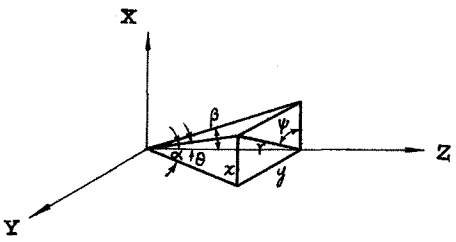

Fig. 7 Correlation between the angular displacements

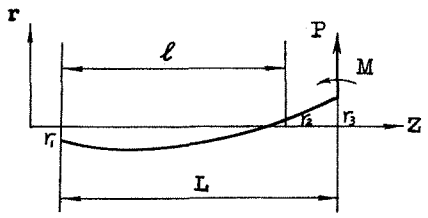

Fig. 8 Elastic curve of the overhung rotor

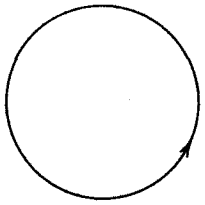

$\bar{e} = 4.712 \quad -0.0484 \quad \frac{Fs}{mg} = 0.5775$

$\bar{\omega} = 1.5 \quad \frac{kyx}{k} = 0.003 \quad \frac{c^*}{k} = 2.417 \times 10^5$

Fig. 9* Orbit of a syn.whirl

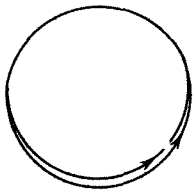

$\bar{\omega} = 1.6 \quad \frac{kyx}{k} = 0.0035 \quad \frac{Fs}{mg} = 0.6571^{**}$

Fig.10 Orbit of a combined whirl

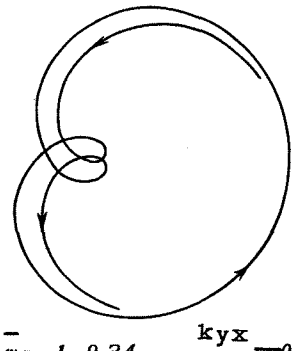

$\bar{\omega} = 1.934 \quad \frac{kyx}{k} = 0.005$

$\frac{Fs}{mg} = 0.9601^{**}$

Fig. 11 Orbit of a combined whirl

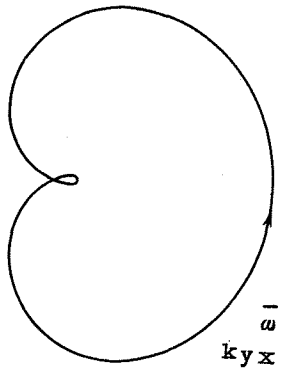

$\bar{\omega} = 2$

$\frac{kyx}{k} = 0.0052$

$\frac{Fs}{mg} = 1.0268^{**}$

Fig.12 Orbit of a combined whirl

** Other Symbols are the same as in fig.9.

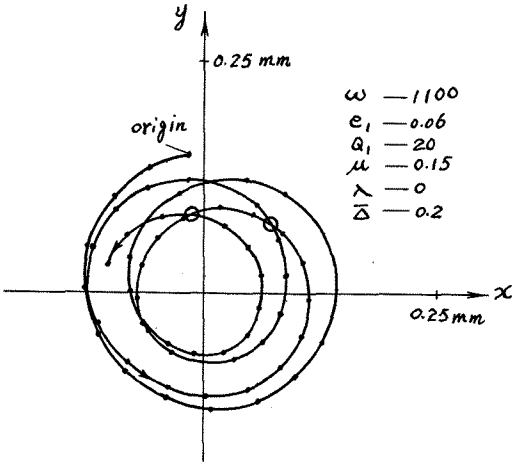

Fig. 13 Orbit of a combined whirl (ω_n 606.3~633)

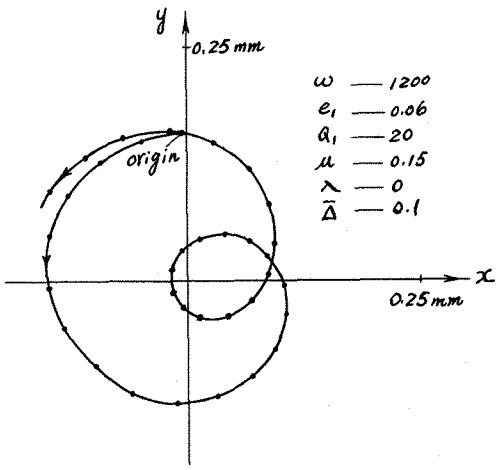

Fig. 14 Orbit of a combined whirl (the amplitude of ½ order component is approaching a steady value on the computer)